Supporting Information for "Limit of validity of Ostwald's rule of stages in a statistical mechanical model of crystallization"

Lester O. Hedges and Stephen Whitelam*
Molecular Foundry, Lawrence Berkeley National Laboratory, 1 Cyclotron Road, Berkeley, CA 94720, USA

SUPPORTING INFORMATION 1: SIMULATION PROTOCOL

We simulated our model using the following grand canonical Metropolis Monte Carlo procedure. This procedure effects a diffusive dynamics and assumes the substrate to be in contact with a thermal bath and a particle bath (i.e we assume the substrate to be in contact with bulk solution). We select at random a lattice site. If that site is occupied by a particle then with probability $p_{\rm del} \leq 1$ we attempt to delete its occupant. We accept this deletion with probability $P_{\rm delete} = \min\left(1, \frac{1}{p_{\rm del}R}\exp\left(-\beta\Delta E - \beta\mu\right)\right)$, where $\beta \equiv 1/(k_{\rm B}T)$ and ΔE is the change of interaction energy following the proposed deletion. With probability $1 - p_{\rm del}$ we instead attempt to change the particle's orientation by ± 1 unit, modulo R (we assume particles to rotate in a plane, and so orientation R neighbors orientation 1). We accept changes of rotation with probability $P_{\rm rotate} = \min\left(1, \exp\left(-\beta\Delta E\right)\right)$. If the chosen site is vacant then we attempt to occupy it with a particle whose orientation is chosen randomly. This attempt succeeds with probability $P_{\rm insert} = \min\left(1, p_{\rm del}R\exp\left(-\beta\Delta E + \beta\mu\right)\right)$. The factors of $p_{\rm del}$ in insertion and deletion rates are required to preserve detailed balance: insertions are *always* attempted if a lattice site is vacant, but deletions are attempted only with probability $p_{\rm del} \leq 1$ if a lattice site is occupied. The factors of R are present for a similar reason: insertion of a particle of a given orientation is attempted with probability $1/R$, but proposing the reverse of that particular insertion occurs with unit probability. We used a lattice of $N = (100)^2$ sites, periodically replicated in each direction.

The basic rate for particle translations (adsorptions and desorptions) is $\sim p_{\rm del}$. The basic rate for particle rotations has two contributions: the first scales as $(1 - p_{\rm del})/(R-1)^2$, and comes from explicit rotation moves; the factor of $(R-1)^2$ accounts for the characteristic time to visit R rotational states. The second contribution scales as $p_{\rm del}/R$, and comes from explicit translations (particles attach to the substrate with randomly-chosen orientations, and so removal and reattachment of a particle allows an effective sampling of its orientation). The first mode of orientation-sampling is most effective in the bulk of a liquidlike cluster, while the second mode operates most readily at the surface of a cluster (where particle detachments are most frequent). There is therefore no constant effective rate at which a cluster explores the configuration space $(N, N_{\rm c})$ shown in Fig. 1. We report values of a parameter $r \equiv (1 - p_{\rm del})/p_{\rm del}$, the relative rate of proposing a rotation or translation.

We set $\mu = -Jz/2 - k_{\rm B}T\ln R$, where $z = 4$ is the coordination number of the lattice. Our choice of μ ensures that, to a mean-field approximation, liquid and vapor phases are equal in free energy. The contribution $-Jz/2$ is the usual Ising model term. The term $-k_{\rm B}T\ln R$ penalizes particles relative to vacancies by an amount that exactly compensates for the entropy difference between particles and vacancies. This choice is motivated by the fact that we consider our simulation protocol to reflect the diffusion of material to and from the substrate, with no change of that material's rotational freedom, rather than to model its creation or destruction (which *would* be accompanied by creation or destruction of rotational entropy). In simulations, orientational correlations in the liquid lower its free energy below that of the vapor.

* swhitelam@lbl.gov

SUPPORTING INFORMATION 2: MEAN-FIELD THEORY

The energy function of our model is $\mathcal{H} = \sum_{i=1}^{N} \left(\frac{1}{2} \sum_j U_{ij} - \mu n_i \right)$, where j runs over the $z = 4$ nearest neighbors of i, and μ is a chemical potential. The variable n_i is 0 if lattice site i is vacant, and is 1 if it is occupied. The pairwise interaction U_{ij} is

$$U_{ij} = -n_i n_j \left(J + Q\delta(s_i, s_j) - Q\tilde{\delta}(s_i, s_j) \right),$$

where $s_i = 1, 2, ..., R$ is the orientation of the particle at lattice site i. The function $\delta(s_i, s_j)$ is 1 if $s_i = s_j$ (aligned particles receive an extra energetic reward), and is zero otherwise. The function $\tilde{\delta}(s_i, s_j)$ is 1 if s_i and s_j are $R/2$ units different, modulo R (antialigned particles receive an energetic penalty), and is zero otherwise.

We can derive the free energy of this model in a mean-field approximation [1, 2] by assuming that each site feels only the thermal average of the fluctuating variables at neighboring sites. The effective interaction at a given site is to this approximation

$$U_{\text{eff}} = -Jzn\langle n \rangle - Qz \sum_{q=1}^{R} n\, \delta(s, q) \left(\langle n\delta(s, q) \rangle - \langle n\tilde{\delta}(s, q) \rangle \right),$$

where we have dropped site labels. By symmetry, all but two terms in the sum over q vanish. The effective free energy per site is then $f_{\text{eff}} = E - TS$, where $E = \frac{1}{2}\langle U_{\text{eff}} \rangle - \mu\langle n \rangle$ and $-TS = k_{\text{B}}T\langle \ln P_{\text{eq}} \rangle$, where $P_{\text{eq}} = \mathrm{e}^{-\beta\mathcal{H}_{\text{eff}}} / \mathrm{Tr}\, \mathrm{e}^{-\beta\mathcal{H}_{\text{eff}}}$ and $\mathcal{H}_{\text{eff}} \equiv U_{\text{eff}} - \mu n$. Thermal averages are defined self-consistently through the relation $\langle A \rangle \equiv \mathrm{Tr}\,(A\, P_{\text{eq}})$. The trace $\mathrm{Tr}(\cdot) \equiv \sum_{n=0,1} \left\{ \delta_{n,1} \sum_{s=1}^{R} + \delta_{n,0} \right\} (\cdot)$ can be carried out by assuming, without loss of generality, the ordering direction to be $s = 1$. We get

$$\begin{aligned} f_{\text{eff}}(\rho, \tau) \;&=\; \frac{1}{2} \left(Jz\rho^2 + Qz\tau^2 \right) \\ &-\; k_{\text{B}}T \ln \left(1 + \mathrm{e}^{\beta(Jz\rho + \mu)} \left[R - 2 + 2\cosh(\beta Qz\tau) \right] \right), \end{aligned} \tag{S1}$$

where $\rho \equiv \langle n \rangle$ is the density and $\tau \equiv \langle n\delta(s, 1) \rangle - \langle n\tilde{\delta}(s, 1) \rangle$ is the crystallinity order parameter. The latter distinguishes disordered fluid phases (for which $\tau = 0$) from the ordered solid phase (for which $\tau \neq 0$). Eq. (S1) is used to derive the mean-field phase diagram and free energy surfaces shown in the main text (Fig. 3), and is used to calculate quantities in Figs. S4–S7.

In our analytic work we have focused on the structure of the bulk free energy landscape, which represents the driving force for crystallization. This landscape accounts only partially for the surface tension between one phase growing in another. To see if this neglect is important one can augment the bulk free energy with surface tension terms, and devise a Cahn-Hilliard-type approximation for the free energy of a growing blob: $F[R(x)] = \int \mathrm{d}^2x\, f_{\text{eff}}(\rho(R(x)), \tau(R(x))) + \frac{K_\rho}{2} (\nabla\rho)^2 + \frac{K_\tau}{2} (\nabla\tau)^2$ (the profile $R(x)$ of the blob can be extracted from Euler-Lagrange equations of the free energy functional). Such calculations confirm qualitatively the trends identified using the bulk free energy surface [W.H. McKerrow, unpublished] (they also allow one to make contact with the classical scaling picture, by approximating $F[R] \sim 2\pi\sigma_{\text{eff}} R - \pi\Delta\mu_{\text{eff}} R^2$).

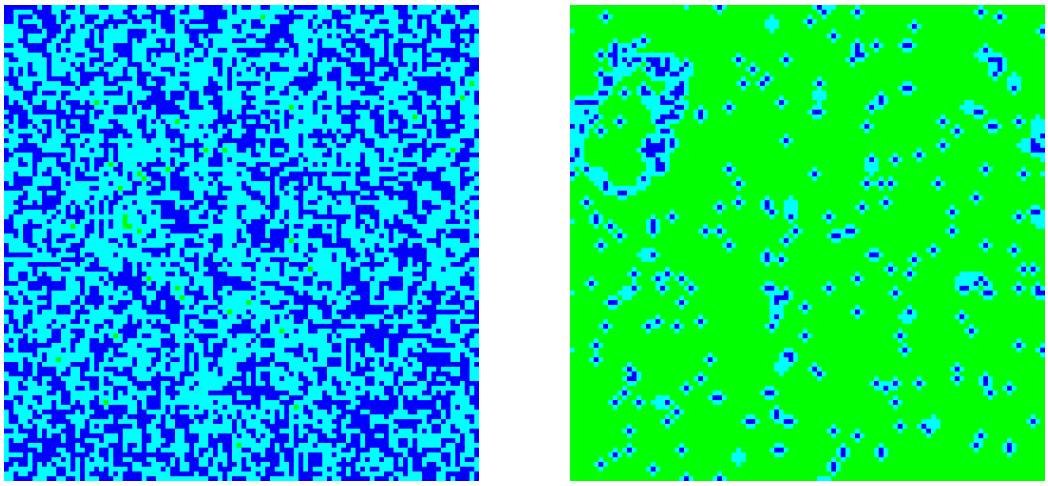

FIG. S1: (Movie) Nucleation pathways from dynamic simulations for slow (left, $r = 0.01$) and fast (right, $r = 99$) rotation rate at point B on the phase diagram (see Fig. 1, main text). Here there is a thermodynamic preference for evolution via a liquidlike critical nucleus. Dynamical trajectories adhere to this preferred pathway: a liquid nucleates on the substrate, and only subsequently does this liquid crystallize. For sluggish rotation rates the liquid consumes the substrate before freezing (upholding Ostwald's rule in a macroscopic sense), while for rapid rotation rates a postcritical but small liquid blob will freeze (upholding Ostwald's rule in a microscopic sense). (To keep file sizes small, the intervals between frames are not equal throughout: at late times we show configurations less frequently.)

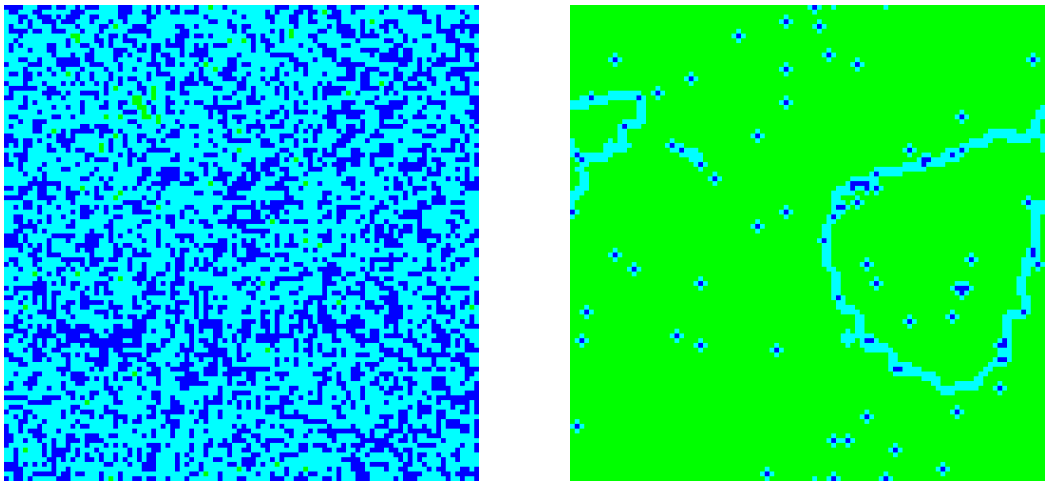

FIG. S2: (Movie) Nucleation pathways from dynamic simulations for slow (left, $r = 0.01$) and fast (right, $r = 99$) rotation rate at point C on the phase diagram (see Fig. 1, main text). Here the thermodynamically-favored pathway is one comprising a crystalline critical nucleus. The indirect pathway with a liquidlike critical nucleus is disfavored by about 5 $k_{\mathrm{B}}T$. Because of this relatively small discrepancy in barrier heights, though, physically meaningful changes of rotation rate can cause dynamical trajectories to follow either pathway. For sufficiently rapid rotation rate (right), the direct pathway is followed. For sluggish rotation rates (left) the indirect pathway is taken. We have shown extremes of relative rotation/translation rate r by way of illustration, but in general changes of dynamical mechanism can be engineered by changes of r comparable to $\exp(\Delta G/k_{\mathrm{B}}T)$, where ΔG is the difference in barrier heights between direct and indirect pathways. (To keep file sizes small, the intervals between frames are not equal throughout: at late times we show configurations less frequently.)

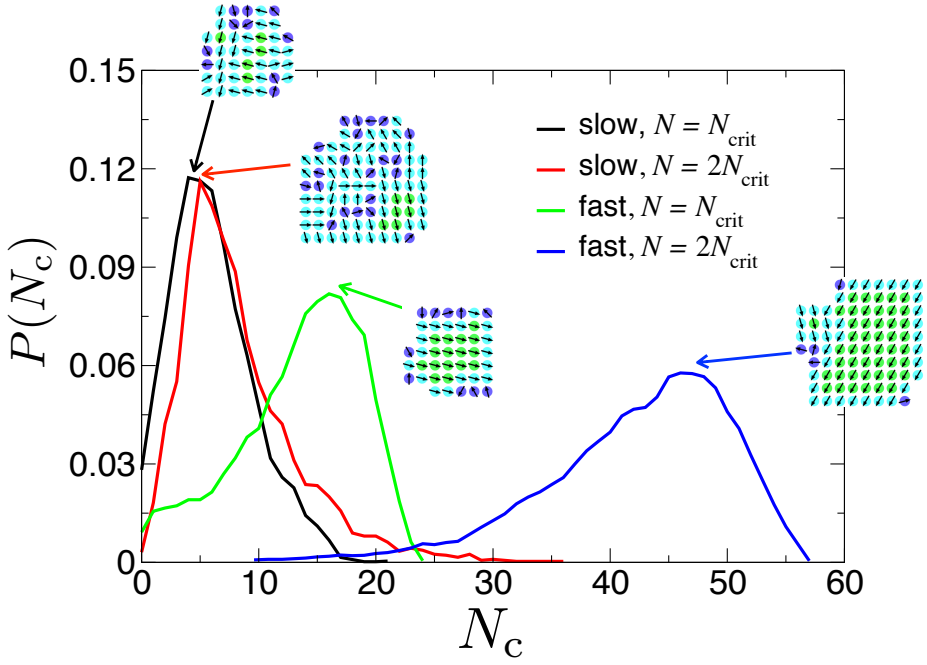

FIG. S3: Distributions of the number of crystalline particles in a cluster, N_c, from dynamical trajectories at phase point C (see Fig. 1, main text). Distributions correspond to clusters at criticality, N_{crit}, and twice the critical size, $2N_{crit}$. For sluggish rotation rates, distributions are peaked at low values of N_c: on average the growing nucleus is liquidlike. For sufficiently rapid rotation rate the direct pathway is preferred. In all cases, trajectories can be observed that buck the trends shown (note the tails of each distribution).

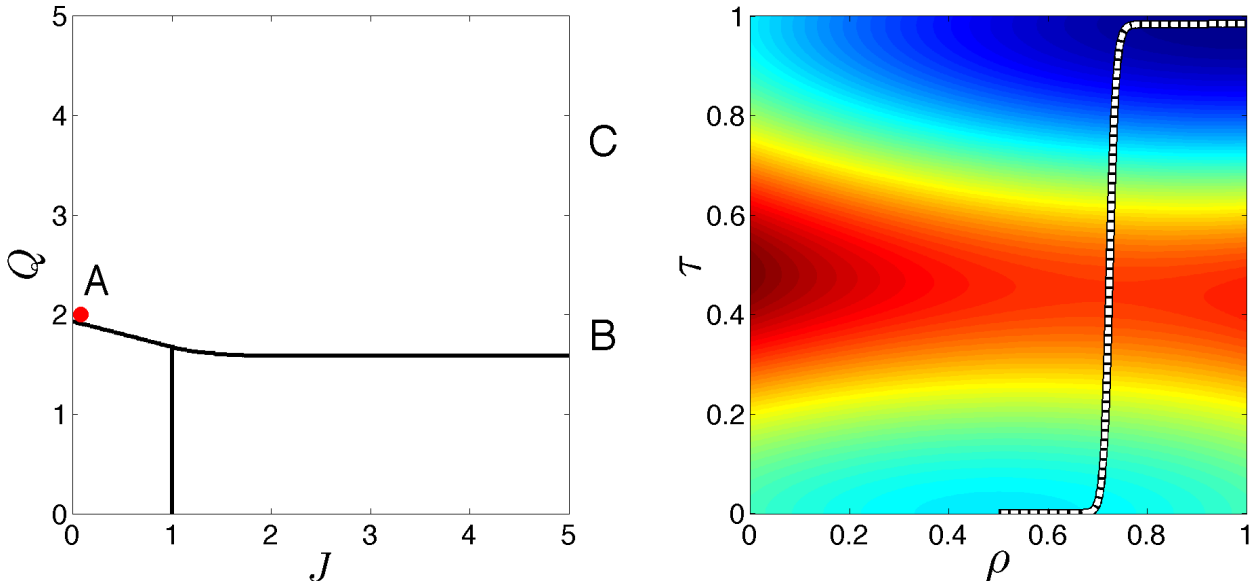

FIG. S4: (Movie) Mean-field phase diagram (left) and free energy surface in a space of density ρ and crystallinity τ as we move in phase space from point A to B and then from B to C. On each free energy surface is plotted the minimum energy pathway from the parent phase (either the homogeneous fluid phase H or the sparse vapor phase V) to the stable solid, which is a measure of the character of the thermodynamic driving force for crystallization. On moving from A to B, this driving force becomes indirect as we approach and cross the demixing line. From B to C, the driving force changes qualitatively as the potency Q of specific binding is increased, and the transition state eventually becomes crystalline once again. These qualitative changes of mechanisms are seen in our simulations.

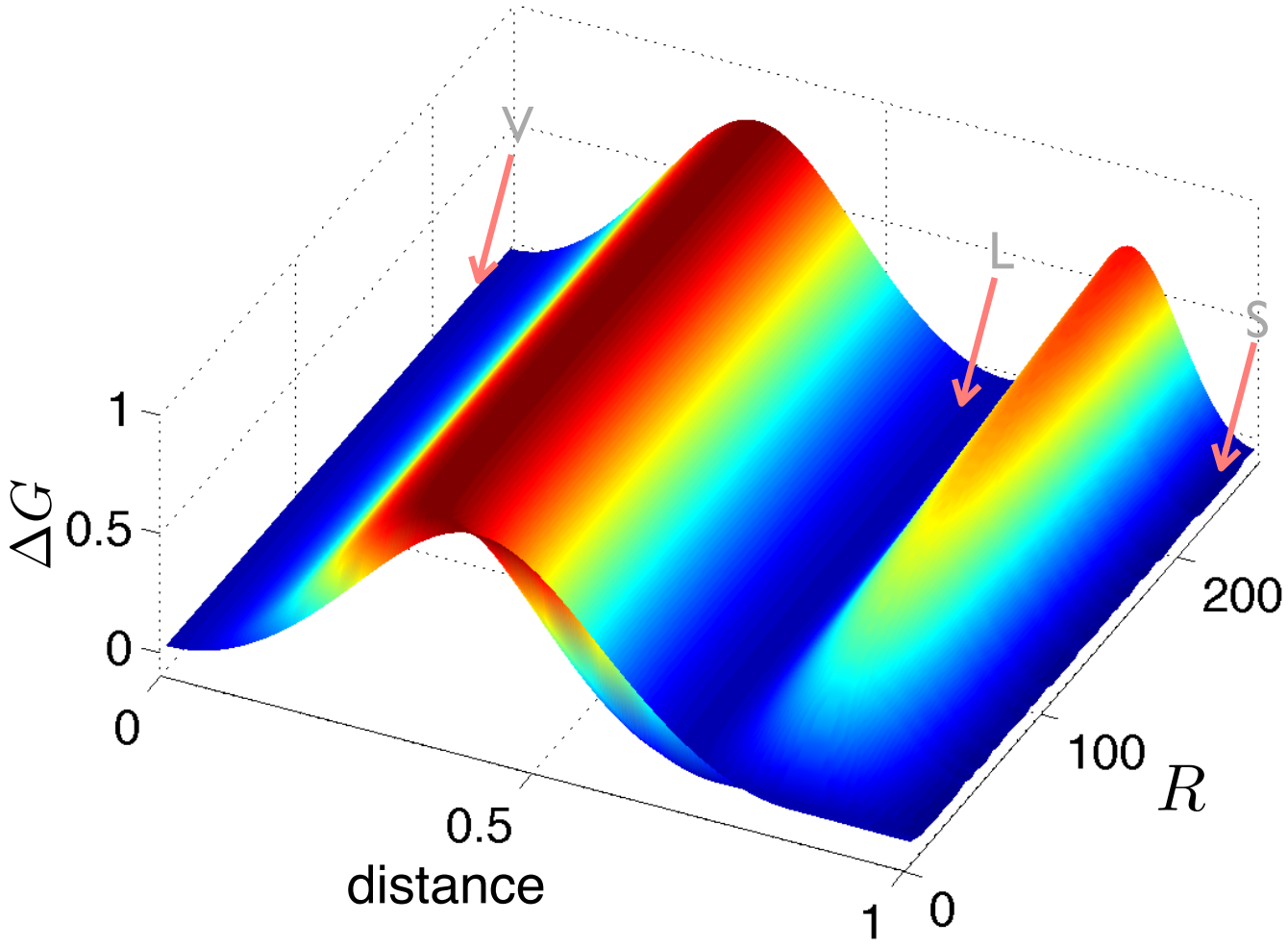

FIG. S5: More detail on the mean-field crystallization landscape. We plot free energy (vertical) along the minimum energy pathway ('distance' axis) of a mean-field free energy surface at $J = 3\,k_{\mathrm{B}}T$, for different values of R. The value of Q is such that we sit just above the freezing line for each R (see point B, previous figure, for $R = 24$). In all cases the pathway observed is an indirect one from vapor (V) to liquid (L) to solid (S). The first barrier seen corresponds to the vapor-to-liquid transformation, and the second to the liquid-to-crystal transformation. Increasing R leads to the growth of a large entropic barrier to crystallization.

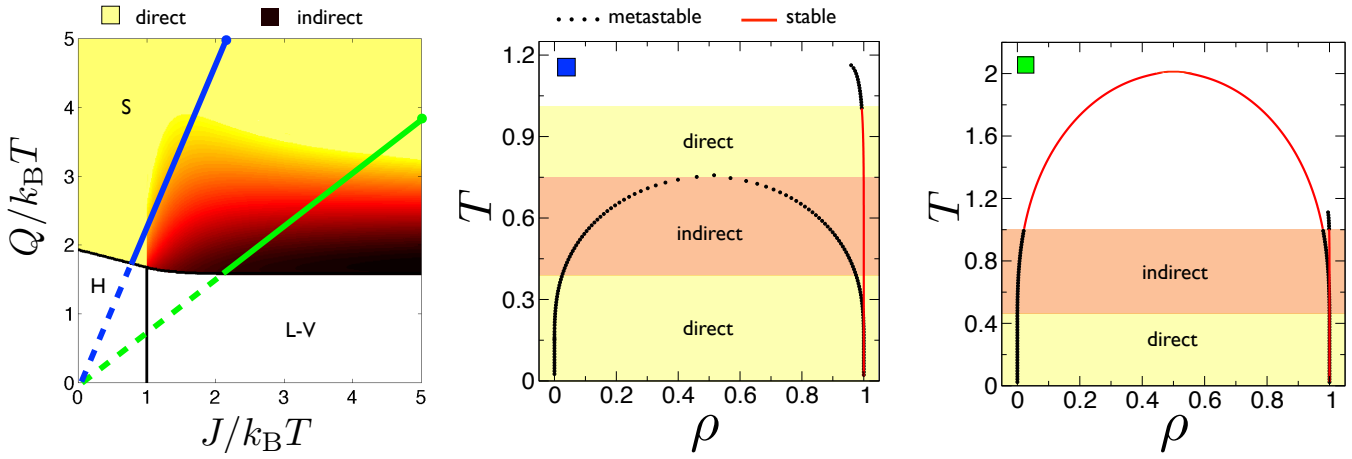

FIG. S6: Temperature is not the direct control of crystallization mechanism. For two different varying-temperature lines ($J/Q = 2.3$ and 0.8) along our mean-field phase diagram (left, $R = 24$), we show phase diagrams in the density (ρ)-temperature (T) plane. These phase diagrams resemble qualitatively those of a protein (middle) or argon (right), with their respective stable- and metastable fluid-fluid demixing critical points [3]. We see that depending on where one lies in parameter space, changing temperature can change the thermodynamically preferred crystallization pathway in a complicated way.

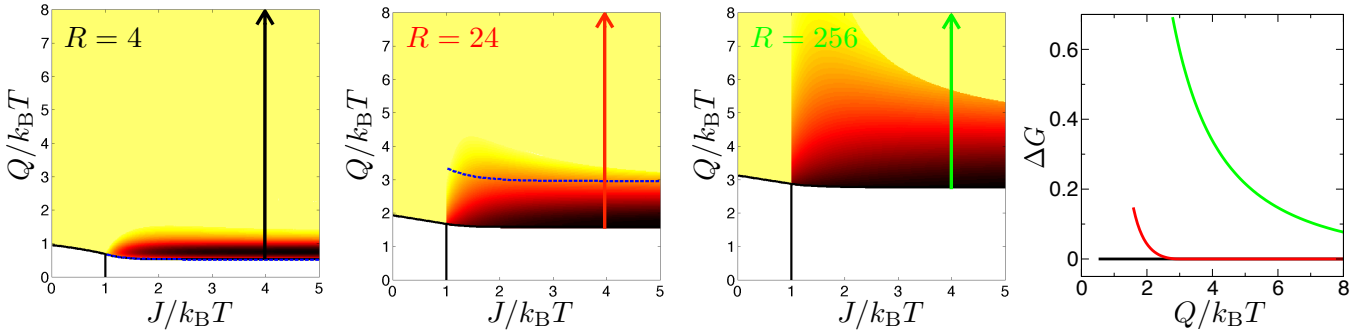

FIG. S7: Supplement to Fig. 3, main text: summarizing the shaping of crystallization landscapes by microscopic parameters. We show mean-field phase diagrams for three values of R, shaded according to where direct (light) and indirect pathways (dark) are favored. Right panel: barrier height ΔG between liquid and crystal phases, as a function of Q, for $J = 4\,k_BT$ (vertical lines on the three diagrams). The change of crystallization driving force from direct to indirect can both preempt (large R) and follow (small R) the loss of liquid metastability.

[1] J. Geng and J. Selinger, Physical Review E **80**, 11707 (2009).
[2] S. Whitelam, J. Chem. Phys. **132**, 194901 (2010).
[3] N. Asherie, A. Lomakin, and G. B. Benedek, Phys. Rev. Lett. **77**, 4832 (1996).